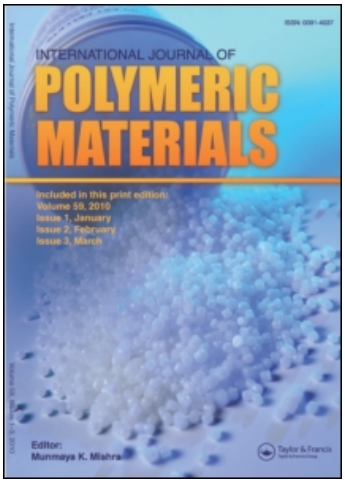

International Journal of Polymeric Materials
Publication details, including instructions for authors and subscription information:
http://www.informaworld.com/smpp/title~content=t713647664

Numerical Simulation of Complex Flows of Semiconcentrated Fiber Suspensions

Seong Jae Lee[a]; Seung Jong Lee[a]
[a] Department of Chemical Engineering, Seoul National University, Seoul, Korea

To cite this Article Lee, Seong Jae and Lee, Seung Jong(1993) 'Numerical Simulation of Complex Flows of Semiconcentrated Fiber Suspensions', International Journal of Polymeric Materials, 21: 1, 65 — 73
To link to this Article: DOI: 10.1080/00914039308048513
URL: http://dx.doi.org/10.1080/00914039308048513

Intern. J. Polymeric Mater., 1993, Vol. 21, pp. 65–73
Reprints available directly from the publisher
Photocopying permitted by license only

Printed in Malaysia

Numerical Simulation of Complex Flows of Semiconcentrated Fiber Suspensions

SEONG JAE LEE and SEUNG JONG LEE*

Department of Chemical Engineering, Seoul National University, Seoul 151-742, Korea

A finite element algorithm has been developed to predict flow and fiber orientation distribution of fiber suspensions.

KEY WORDS Flow simulation, fiber orientation, fiber suspensions.

1. INTRODUCTION

Mechanical properties of short fiber reinforced composite materials strongly depend on the orientation distribution of fibers in the final products, which in turn is determined by the history of the flow field experienced during the processing steps. And the flow field itself is also influenced by the orientation distribution of fibers. Therefore, it is important to understand the complicated flow patterns of fiber suspensions through complex geometries and to predict the orientation distribution of fibers.

Most analytical studies of the fiber motion within the fluid flow have been based on Jeffery's early model,[1] which described the motion of an ellipsoid immersed in a Newtonian suspending medium. This model can be only applied to dilute suspensions since the interactions among ellipsoids and between ellipsoid and fluid were neglected in the model. Quantitative analyses for predicting the orientation of ellipsoids in a variety of flow situations have been given in the numerous studies by Goldsmith and Mason.[2] Givler *et al.*[3] have developed a numerical simulation scheme to predict the fiber orientation in various geometries by integrating Jeffery's equation along the streamlines. Folgar and Tucker[4] proposed a phenomenological model which can represent the interaction between fibers for concentrated fiber suspensions by adding a diffusion term into Jeffery's equation; then Jackson *et al.*[5] applied this model to predict the fiber orientation in the compression molding process.

In an attempt to consider the interaction between fluid and fiber, Batchelor[6] derived the bulk stress tensor in a dilute suspension of rigid ellipsoids as an ensemble average when the suspension is statistically homogeneous. Lipscomb *et al.*[7] was the first to consider the fluid/fiber interaction in the numerical simulation of the flow of fiber suspensions in contraction geometries using the full alignment assumption for the fiber orientation distribution. While their simulation and experimental

results have shown that the full alignment assumption is valid in dilute suspensions, the orientation distribution of the fiber should be obtained for more accurate and advanced calculations.

The concept of the orientation distribution function (ψ) had long been used to represent the state of the fiber orientation, but using ψ is too time-consuming for numerical calculations of the fiber orientation complex flows. The concept of the orientation tensor as a compact form of the orientation description, used by Advani and Tucker,[8,9] is very convenient and efficient for this purpose. So far, there has not been any studies which solve simultaneously the coupled system of equations for the flow and the orientation distribution numerically. In this work, we have developed a rigorous numerical scheme to predict two-dimensional flow and orientation distribution in the flow of fiber suspensions through contraction geometries including the fiber/fiber and fluid/fiber interactions using the finite element method.

2. MATHEMATICAL MODELING AND GOVERNING EQUATIONS

The flow and fiber orientation distribution in the steady isothermal flow of fiber suspensions through contraction geometries are governed by the following equations:

(Continuity Equation)

$$\nabla \cdot v = 0 \tag{1}$$

(Cauchy Momentum Equation)

$$-\nabla p + \nabla \cdot T + f = \rho v \cdot \nabla v \tag{2}$$

The extra stress tensor T is given by the constitutive equation for the fiber suspensions. The continuum model approach to formulating the constitutive equation is based on the works of Batchelor[6] and Hinch and Leal[10] and the model for the dilute and semiconcentrated fiber suspensions leads to the following form of the constitutive equation.

$$T = 2\mu D + 2\mu\phi\{C_1 D: \langle pppp\rangle + C_2(D\cdot\langle pp\rangle + \langle pp\rangle\cdot D) + C_3 D\} \tag{3}$$

Here, μ is the viscosity of the Newtonian suspending medium, D is the rate of deformation tensor, defined by $D = (\nabla v + \nabla v^T)/2$, ϕ is the volume fraction of the fiber, p is the unit vector along the axis of the fiber, and $\langle\ \rangle$ denotes the integral over all p weighted by the orientation distribution function of the fiber, that is,

$$\langle pp\rangle = \int pp\psi(p)\, dp \tag{4a}$$

$$\langle pppp\rangle = \int pppp\psi(p)\, dp \tag{4b}$$

The stress shape coefficients C_1, C_2, and C_3, determined by the aspect ratio of the fiber (r), are expressed as follows in the limiting case of $r >> 1$.

$$C_1 = \frac{r^2}{2[\ln(2r) - 1.5]} \tag{5a}$$

$$C_2 = \frac{6 \ln 2r - 11}{r^2} \tag{5b}$$

$$C_3 = 2 \tag{5c}$$

Furthermore, for large r this continuum constitutive model, Equation (3), reduces to

$$T = 2\mu D + \mu\alpha D:\langle pppp\rangle \tag{6a}$$

$$\alpha = \phi \frac{r^2}{\ln(2r) - 1.5} \tag{6b}$$

Besides the above equations, the equation for the fiber orientation is required; it can be given in terms of the orientation tensors defined by Equation (4):

$$v\cdot\nabla a_2 = -W\cdot a_2 + a_2\cdot W + \lambda(D\cdot a_2 + a_2\cdot D - 2D:a_2\cdot a_2) + 2C_I\dot{\gamma}(I - \nu a_2) \tag{7}$$

Here, a_2 represents the second order orientation tensor $\langle pp\rangle$ given by Equation (4a), and the quadratic closure approximation to the fourth order orientation tensor has been applied, that is, $a_4 = \langle pppp\rangle = a_2\cdot a_2$. Note that the last term in Equation (7) represents a diffusion term to account for the fiber/fiber interaction, whose magnitude is controlled by a phenomenological interaction coefficient C_I.

The geometry of interest in this study is the axisymmetric 4.5:1 contraction. This

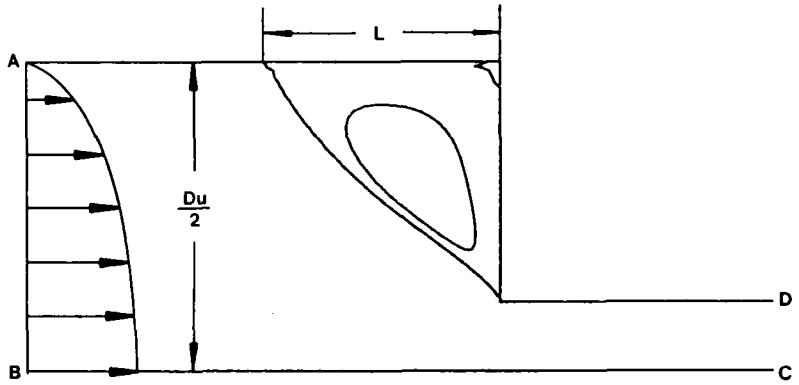

FIGURE 1 Contraction geometry used in this study.

geometry has been chosen since there already exists the corresponding experimental data of Lipscomb *et al.*[7] A schematic diagram and boundary conditions for the contraction geometry is illustrated in Figure 1. Only the half domain of the system is considered because of its symmetry. The inlet velocity profile at the entrance (along A-B) is assumed to be fully developed Poiseuille flow. The centerline (along B-C) is a boundary which has a symmetric character. Thus the radial velocity and the axial velocity gradient in the radial direction is zero along this line. The force free boundary condition is assumed at the outlet. Along the solid wall (along D-A), a no-slip boundary condition is applied. The boundary condition for the fiber orientation is only required at the inlet (along A-B) because the orientation equation is a first order hyperbolic type of PDE, and a random fiber orientation distribution is assumed. For a two-dimensional orientation distribution, it is given by $a_{11} = a_{22} = 0.5$ and $a_{12} = 0$.

3. NUMERICAL METHODS

In this work, the standard Galerkin finite element method has been used to solve the flow and orientation equations, Equations (1), (2), (6), and (7). The velocity components u and v (r and z directions, respectively), the pressure p, and the orientation tensor components a_{11} and a_{12} are approximated in terms of the following shape functions

$$\begin{aligned} u &= \sum u_j\psi_j, \qquad v = \sum v_j\psi_j, \qquad p = \sum p_j\phi_j, \\ a_{11} &= \sum a_{11j}\psi_j, \qquad a_{12} = \sum a_{12j}\psi_j \end{aligned} \tag{8}$$

where u_j, v_j, p_j, a_{11j}, and a_{12j} are nodal values of velocity components, pressure, and orientation tensor components; ψ_j is either a 6-node quadratic shape function in the triangular elements or a 9-node biquadratic shape function in the quadrilateral elements; and ϕ_j is either a 3-node linear shape function in the triangular elements or a 4-node bilinear shape function in the quadrilateral elements.

Using the divergence theorem to the momentum equation, the Galerkin forms of the momentum equations are given as follows:

$$\langle r\psi_{i,1};\ -p + T_{11}\rangle + \langle r\psi_{i,2};\ T_{12}\rangle + \langle \psi_i;\ T_{33}\rangle - \langle \psi_i p\rangle = \langle\langle r\psi_i;\ t_1\rangle\rangle \tag{9a}$$

$$\langle r\psi_{i,1};\ T_{12}\rangle + \langle r\psi_{i,2};\ -p + T_{22}\rangle = \langle\langle r\psi_i;\ t_2\rangle\rangle \tag{9b}$$

Here, the 1-, 2-, and 3-directions are associated with r, z, and θ directions, $\langle;\rangle$ stands for the integration over the domain, $\langle\langle;\rangle\rangle$ stands for the integration along the boundary surface, and t_1 and t_2 are the r and z components of the contact force per unit area on the boundary. The integration schemes used here are 9-point Gaussian quadrature in the quadrilateral elements and 7-point Gaussian quadrature

in the triangular elements. And T_{ij} are given by the constitutive equation, Equation (6), as

$$T_{11} = 2\mu u_{,1} + \mu\alpha\{a_{11}a_{11}u_{,1} + a_{11}a_{12}(u_{,2} + v_{,1}) + a_{11}(1 - a_{11})v_{,2}\} \tag{10a}$$

$$T_{12} = \mu(u_{,2} + v_{,1}) + \mu\alpha\{a_{11}a_{12}u_{,1} + a_{12}a_{12}(u_{,2} + v_{,1}) + a_{12}(1 - a_{11})v_{,2}\} \tag{10b}$$

$$T_{22} = 2\mu v_{,2} + \mu\alpha\{a_{11}(1 - a_{11})u_{,1} + a_{12}(1 - a_{12})(u_{,2} + v_{,1}) + (1 - a_{11})(1 - a_{11})v_{,2}\} \tag{10c}$$

$$T_{33} = 2\mu u/r \tag{10d}$$

With the weight function ϕi, the continuity equation becomes

$$\langle r\phi i;\ u_{,1} + u/r + v_{,2}\rangle = 0 \tag{11}$$

And with the weight function ψ_i, the orientation equations are given as follows

$$\langle \psi_i;\ ua_{11,1} + va_{11,2}\rangle = -\langle \psi_i;\ 2\omega_{12}a_{12}\rangle + [\psi_i;\ \lambda[2d_{11}a_{11} + 2d_{12}a_{12} - 2\{d_{11}a_{11}a_{11} + 2d_{12}a_{12}a_{11} + d_{22}(1 - a_{11})a_{11}\}] + 2C_I\dot{\gamma}(1 - 2a_{11})\rangle \tag{12a}$$

$$\langle \psi_i;\ ua_{12,1} + va_{12,2}\rangle = \langle \psi_i;\ 2\omega_{12}a_{11} - \omega_{12}\rangle + \langle \psi_i;\ \lambda[d_{11}a_{12} + d_{12} + d_{22}a_{12} - 2\{d_{11}a_{12}a_{11} + 2d_{12}a_{12}a_{12} + d_{22}(1 - a_{11})a_{12}\}] - 4C_I\dot{\gamma}a_{12}\rangle \tag{12b}$$

where

$$\dot{\gamma} = [2(d_{11}^2 + d_{22}^2 + d_{33}^2 + 2d_{12}^2)]^{0.5} \tag{13}$$

By substituting the approximations of Equation (8) into Equations (9) and (12), a nonlinear algebraic system of equations is obtained which must be solved by an iterative technique. Equations (9) and (11) are solved first for Newtonian creeping flow at $\alpha = 0$. Then, using this creeping flow solution, Equation (12) is solved for a_{11} and a_{12} at $\alpha > 0$ and this solution is again used to solve Equations (9) and (11) for the velocity and pressure. This procedure is repeated until the convergence is obtained at a given value of α and then the value of α is increased gradually to obtain the solutions at higher α values of interest.

4. RESULTS AND DISCUSSION

The meshes used in this work to simulate the flow of fiber suspensions through axisymmetric 4.5:1 contraction geometry are shown in Figure 2. MESH1 is made of 135 elements and MESH2 contains 540 elements. The conditions used in the simulations are those of Lipscomb *et al.*[7] That is, the value of α in this work is set

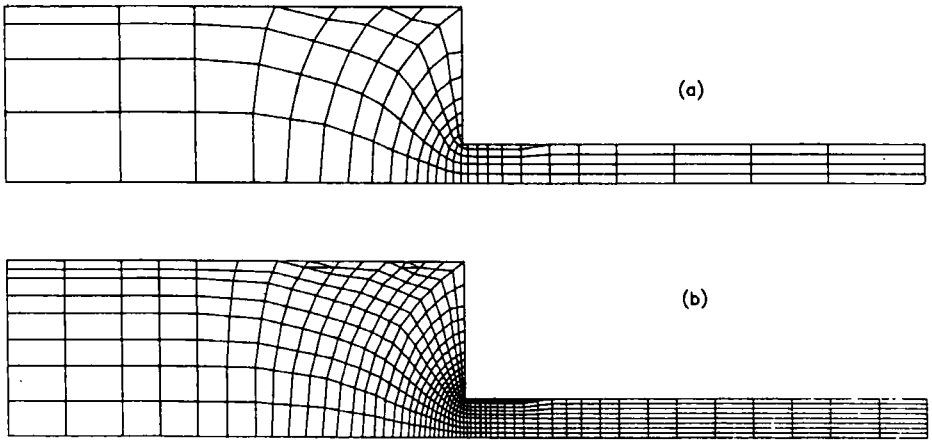

FIGURE 2 Finite element meshes, (a) MESH1; (b) MESH2.

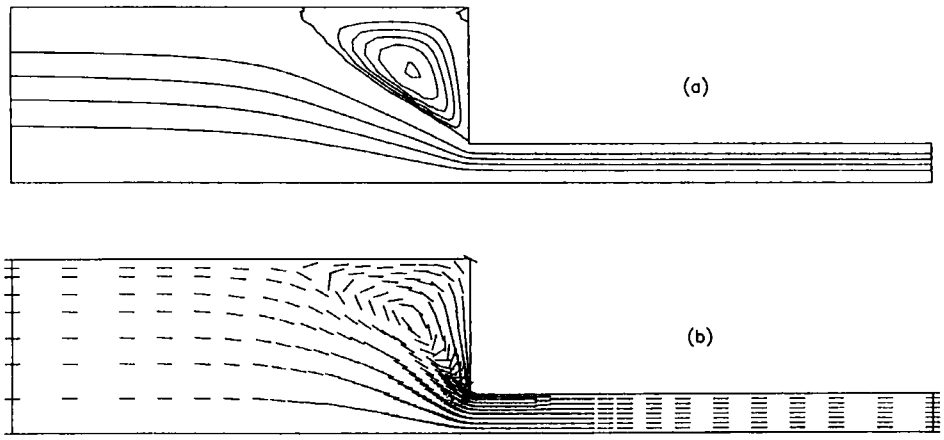

FIGURE 3 (a) Streamlines and (b) fiber orientation distribution obtained at $\alpha = 7.12$ with full alignment assumption on MESH1.

at 7.12, since the aspect ratio of fiber was 276 and the fiber volume fraction 0.00045 in their experiments.

The streamlines and orientation distribution at $\alpha = 7.12$ on MESH1 using the full alignment assumption is given in Figure 3. This full alignment assumption, which neglects fiber//fiber interaction, has been used by Lipscomb *et al.*[7] and it results in the maximum vortex size at the corner. The vortex size in Figure 3 is somewhat larger than the experimental one and it implies that there may exist interaction among fibers in the experiments.

Figure 4 represents the results at $\alpha = 7.12$ and $C_I = 0.1$ on MESH1. As expected, the vortex size at the corner becomes smaller, even smaller than the experimental one. Therefore, the value of C_I needs to be reduced to obtain a vortex size consistent with the experiment. As C_I decreases, the convergence of the iterative numerical scheme is difficult to obtain. In Figure 5, the results are shown for $C_I = 0.056$,

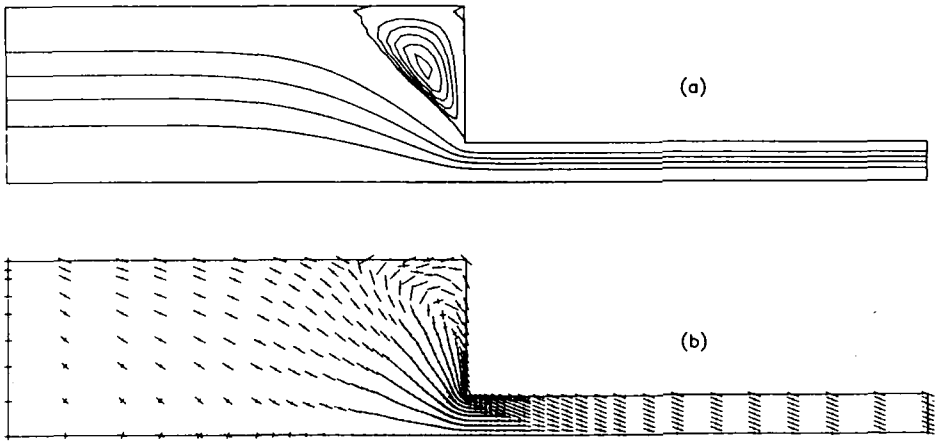

FIGURE 4 (a) Streamlines and (b) fiber orientation distribution obtained at $\alpha = 7.12$ and $C_I = 0.1$ on MESH1.

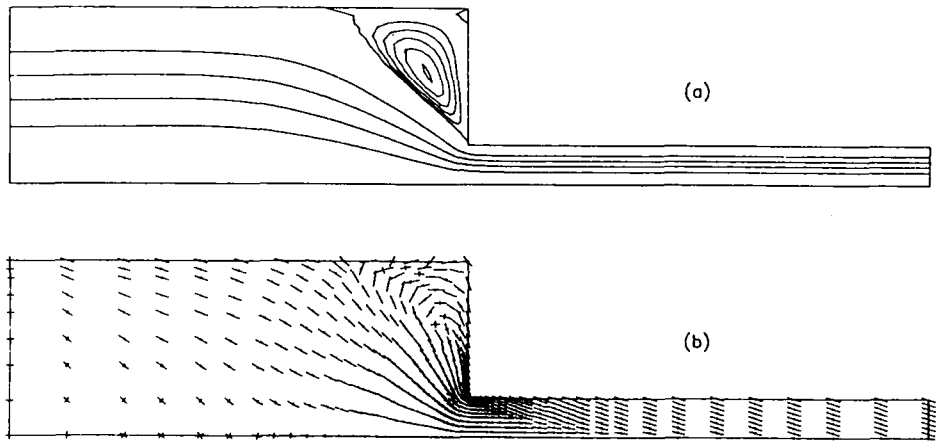

FIGURE 5 (a) Streamlines and (b) fiber orientation distribution obtained at $\alpha = 7.12$ and $C_I = 0.056$ on MESH1.

the smallest value of C_I attainable on MESH1. But the vortex size in Figure 5 is still smaller than the experimental one. A finer mesh (MESH2) is then used to reduce the value of C_I further, and convergence is attained down at $C_I = 0.029$ on MESH2, whose results are shown in Figure 6. To overcome this convergence problem at low values of C_I, the streamline-upwind method[11] may be used to treat the convective terms in the orientation equations. Marchal and Crochet[12] have successfully applied this method to the viscoelastic flow problems.

In order to represent the orientation distribution graphically, two eigenvectors of the orientation tensor whose magnitudes are given by the corresponding eigenvalues may be drawn. Those two major and minor axes give an orientation ellipsoid which indicates the degree of orientation distribution along every direction. The calculated eigenvectors are also shown in Figures 3–6 to show the orientation

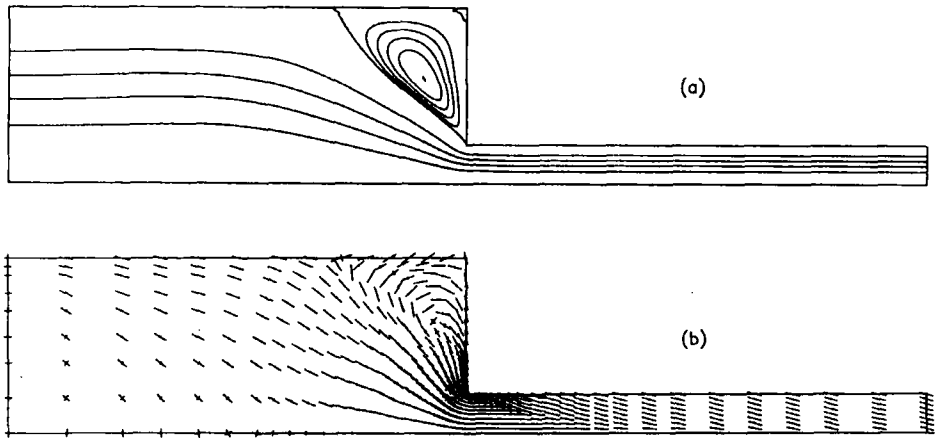

FIGURE 6 (a) Streamlines and (b) fiber orientation distribution obtained at $\alpha = 7.12$ and $C_I = 0.029$ on MESH2.

distribution of fibers. In Figure 3, fibers align fully along the streamlines due to the full alignment assumption, and Figures 4–6 illustrate the fiber orientation distribution obtained at $C_I > 0$. Along the centerlines in Figures 4–6, the fibers remain almost randomly positioned until the vicinity of the contraction region, where they start to align along the flow direction. Along the wall boundary, fibers quickly distribute to their own orientation, and the orientations are always constant over the shear field except for the recirculating vortex region. Because the orientation distribution is a function of total shear, fibers along the wall have the steady state distribution of the infinite shear at a given C_I.

5. CONCLUSIONS

A finite element algorithm has been developed to predict the flow and fiber orientation distribution of fiber suspensions through contraction geometry, considering the fluid/fiber and fiber/fiber interaction simultaneously. The flow of fiber suspensions is quite different from that of the suspending Newtonian medium without fibers, and the most probable directions of fiber orientation distributions are also quite different from the streamline directions, especially in the shear flow region.

The maximum vortex size is observed when the full alignment assumption is used, but the vortex size decreases as the interaction coefficient C_I increases. Numerical results compared with the experimental results of Lipscomb *et al.* within reasonable agreement.

The problem of constitutive models to treat the concentrated suspensions and the calculation for the entire range of the interaction coefficient will require further study.

Acknowledgment

This research has been supported by Lucky Ltd.

References

1. G. B. Jeffery, *Proc. Roy. Soc.*, **A102**, 161 (1923).
2. H. Goldsmith and S. G. Mason, In: *Rheology: Theory and Applications*, ed. . R. Eirich, Academic Press, 1967.
3. R. C. Givler, M. J. Crochet and R. B. Pipes, *J. Compos. Mat.*, **17**, 330 (1983).
4. F. P. Folgar and C. L. Tucker, *J. Reinf. Plast. Compos.*, **3**, 98 (1984).
5. W. C. Jackson, S. G. Advani and C. L. Tucker, *J. Compos. Mat.*, **20**, 539 (1986).
6. G. K. Batchelor, *J. Fluid Mech.*, **41**, 545 (1970), **44**, 419 (1970).
7. G. G. Lipscomb, M. M. Denn, D. U. Hur and D. V. Boger, *J. Non-Newtonian Fluid Mech.*, **26**, 297 (1988).
8. S. G. Advani and C. L. Tucker, *J. Rheol.*, **31**, 751 (1987).
9. S. G. Advani and C. L. Tucker, *ANTEC '88*, 687 (1988).
10. E. J. Hinch and L. G. Leal, *J. Fluid Mech.*, **52**, 683 (1972).
11. A. N. Brooks and T. J. R. Hughes, *Comp. Meth. Appl. Mech. Eng.*, **32**, 199 (1982).
12. J. M. Marchal and M. J. Crochet, *J. Non-Newtonian Fluid Mech.*, **26**, 77 (1987).